Preconditioned Iterative Methods for High-resolution Image Reconstruction with Multisensors

Raymond H. Chan[a], Tony F. Chan[b], Michael K. Ng[c],
Wun-Cheung Tang[a], and Chiu-Kwong Wong[b]

[a]Department of Mathematics, The Chinese University of Hong Kong
Shatin, Hong Kong, P.R. China

[b]Department of Mathematics, University of California, Los Angeles
405 Hilgard Avenue, Los Angeles, CA 90095-1555

[c]Department of Mathematics, The University of Hong Kong
Pokfulam Road, Hong Kong, P.R. China

ABSTRACT

We study the problem of reconstructing a high-resolution image from multiple undersampled, shifted, degraded frames with subpixel displacement errors. The corresponding reconstruction operator $\mathcal{H}$ is a spatially variant operator. In this paper, instead of using the usual zero boundary condition (corresponding to a dark background outside the scene), the Neumann boundary condition (corresponding to a reflection of the original scene at the boundary) is imposed on the images. The resulting discretization matrix of $\mathcal{H}$ is a block-Toeplitz-Toeplitz-block-like matrix. We apply the preconditioned conjugate gradient (PCG) method with cosine transform preconditioners to solve the discrete problems. Preliminary results show that the image model under the Neumann boundary condition gives better reconstructed high-resolution images than that under the zero boundary condition, and the PCG method converges very fast.

Keywords: block-Toeplitz-Toeplitz-block-like matrix, preconditioned conjugate gradient, cosine transform preconditioner, regularization, high-resolution image reconstruction, Neumann boundary condition

1. INTRODUCTION

High-resolution image reconstruction has many electronic imaging applications, including aerial or facilities surveillance, consumer, commercial, medical, forensic, and scientific imaging. The observed images often have low resolution and degraded by blur and noise. Increasing the image resolution by using digital signal processing technique[2,6–8,10,12] is therefore of great interest.

We consider the reconstruction of a high resolution image f from multiple undersampled, shifted, degraded and noisy images. Multiple undersampled images are often obtained by using multiple identical image sensors shifted from each other by subpixel displacements. If the image sensor arrays are shifted from each other by an exact subpixel displacement in the ideal case, then the task of reconstructing high resolution images reduces to solving a spatially invariant linear system, $\mathcal{H}_0 f = g$. Here g, the so-called *observed high-resolution image*, is a combination of all the low-resolution frames. However, exact subpixel displacements are not practical, and we usually obtain a spatially variant system $\mathcal{H} f = g$ instead.

Since the system is ill-conditioned and generally not positive definite, we solve it by using a minimization and regularization technique:

$$\min_f \left\{ \|\mathcal{H} f - g\|_2^2 + \alpha \mathcal{R}(f) \right\}. \tag{1}$$

Here $\mathcal{R}(f)$ is a functional which measures the regularity of f and the regularization parameter α is used to control the degree of regularity of the solution. Previous works (for instance Bose and Boo[2]) did not emphasize the boundary condition of the problem (1). Since we do not have any information about the scene outside the frames, a natural approach is to impose zero boundary condition outside the scene, i.e., assuming a dark background outside the scene.[1] However, when this assumption is not satisfied by the images, ringing effect will occur at the boundary of

the reconstructed image (see the numerical results in Bose and Boo[2]). The problem is more severe if the image is reconstructed from a large sensor array since the number of pixel values of the image affected by the sensor array increases. We here propose using the Neumann boundary condition on the image, which assumes that the scene immediately outside is a reflection of the original scene at the boundary. Our numerical results show that the error of the image under the Neumann boundary condition is less than that under the zero boundary condition.

The discretization matrix of $\mathcal{H}$ is a block-Toeplitz-Toeplitz-block-like matrix. The preconditioned conjugate gradient (PCG) method is commonly used in solving the system, see Chan and Ng.[4] We observe that for a 2×2 sensor array with exact subpixel displacement, the matrix can be diagonalized by the discrete cosine transform matrix. We thus propose using the PCG method with cosine transform preconditioners for solving the system. Numerical results show that our preconditioners perform significantly better than other preconditioners.

The main results of this paper is to propose (i) a novel approach of using Neumann boundary conditions for image reconstruction and (ii) PCG methods with cosine transform based preconditioners to solve large linear systems arising from image reconstruction. In Section 2, we give a mathematical formulation of the problem. The Neumann boundary condition and a brief introduction on cosine transform preconditioners will be given there. Finally, numerical results are given in Section 3.

2. HIGH-RESOLUTION IMAGE RECONSTRUCTION

2.1. Mathematical Model

Suppose we have an $L_1 \times L_2$ sensor array, each sensor has $N_1 \times N_2$ sensing elements, and the size of each sensing element is $T_1 \times T_2$. Our aim is to reconstruct an image of resolution $M_1 \times M_2$, where $M_1 = L_1 \times N_1$ and $M_2 = L_2 \times N_2$. The sampled base interval for the high-resolution image is therefore equals to $T_1/L_1 \times T_2/L_2$. To maintain the aspect ratio of the reconstructed image, we consider the case where $L_1 = L_2 = L$ only.

In order to have enough information to resolve the high resolution image, there are subpixel displacements between the sensors. In the ideal case, the sensors are shifted from each other by a value proportional to the sampled base interval $T_1/L \times T_2/L$. However, in practice there can be small perturbations around the ideal subpixel locations due to imperfection of the mechanical imaging system. Thus, for $l_1, l_2 = 0, 1, \cdots, L-1$ with $(l_1, l_2) \neq (0,0)$, the horizontal and vertical displacements $d^x_{l_1 l_2}$ and $d^y_{l_1 l_2}$ are given by

$$d^x_{l_1 l_2} = \frac{T_1}{L}(l_1 + \epsilon^x_{l_1 l_2}) \quad \text{and} \quad d^y_{l_1 l_2} = \frac{T_2}{L}(l_2 + \epsilon^y_{l_1 l_2}),$$

where $\epsilon^x_{l_1 l_2}$ and $\epsilon^y_{l_1 l_2}$ denote respectively the normalized horizontal and vertical displacement errors. Here we assume that

$$|\epsilon^x_{l_1 l_2}| < \frac{1}{2} \quad \text{and} \quad |\epsilon^y_{l_1 l_2}| < \frac{1}{2}.$$

Since these can be set by users during camera calibration, the parameters $\epsilon^x_{l_1 l_2}$ and $\epsilon^y_{l_1 l_2}$ may be assumed to be known. We remark that the displacement errors cannot be greater than or equal to $1/2$ since the image sensor arrays are shifted from each other described by the rectangularly sampled base interval $T_1/L \times T_2/L$.

Let f be the original scene, the observed low-resolution image $g_{l_1 l_2}$ for the (l_1, l_2)-th sensor is modeled by:

$$g_{l_1 l_2}[n_1, n_2] = \int_{T_2(n_2 - \frac{1}{2}) + d^y_{l_1 l_2}}^{T_2(n_2 + \frac{1}{2}) + d^y_{l_1 l_2}} \int_{T_1(n_1 - \frac{1}{2}) + d^x_{l_1 l_2}}^{T_1(n_1 + \frac{1}{2}) + d^x_{l_1 l_2}} f(x_1, x_2) dx_1 dx_2 + \eta_{l_1 l_2}[n_1, n_2], \tag{2}$$

for $n_1 = 1, \ldots, N_1$ and $n_2 = 1, \ldots, N_2$. Here $\eta_{l_1 l_2}$ is the noise corresponding to the (l_1, l_2)-th sensor. We intersperse the low-resolution images to form an $M_1 \times M_2$ image by assigning

$$g[L(n_1 - 1) + l_1, L(n_2 - 1) + l_2] = g_{l_1 l_2}[n_1, n_2].$$

Here g is an $M_1 \times M_2$ image and is called the *observed high-resolution image*. Figure 1 shows the method of forming a 4×4 image g with a 2×2 sensor array each having a 2×2 sensing elements ($L = 2$, $M_1 = M_2 = 4$, $N_1 = N_2 = 2$ and $T_1 = T_2 = 2$).

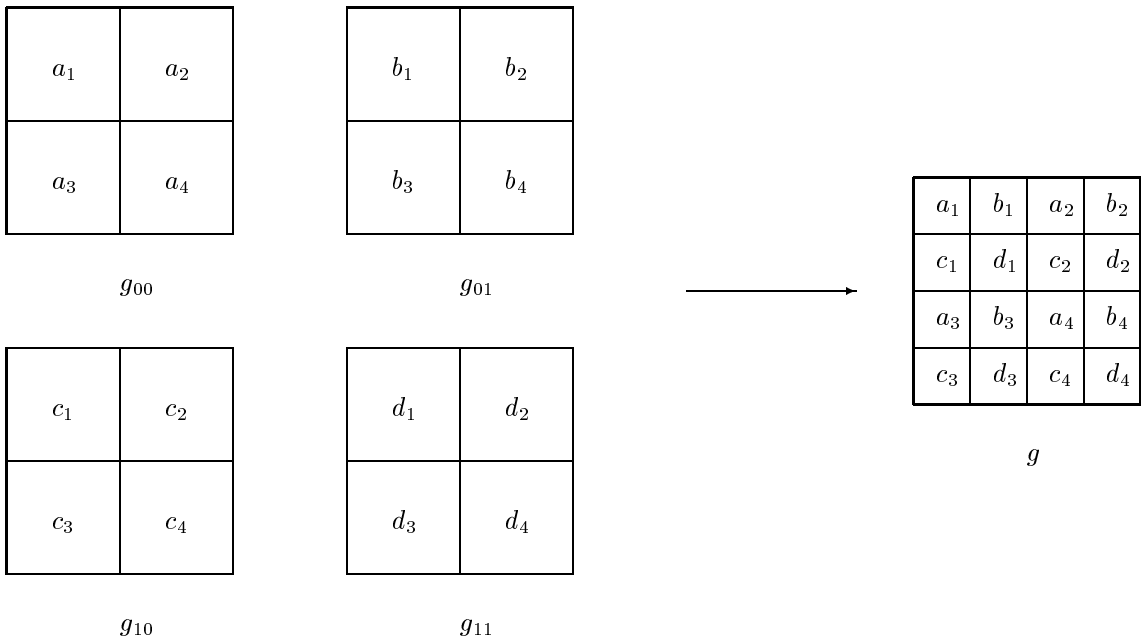

Figure 1. Construction of the observed high-resolution image

Using a lexicological ordering for g, we obtain

$$g = \mathcal{H}f + \eta$$

where $\mathcal{H}$ is a spatially variant operator[2] . Since $\mathcal{H}$ is ill-conditioned due to averaging of pixel values in the image model in (2), classical Tikhonov regularization is used and the minimization problem (1) is solved. In this paper, we use regularization functionals:

$$\mathcal{R}(f) = \|f\|_2^2 \quad \text{and} \quad \mathcal{R}(f) = \|\mathcal{D}f\|_2^2$$

where $\mathcal{D}$ is the first order differential operator. In these cases, the Euler-Lagrange equation of (1) becomes

$$(\mathcal{H}^*\mathcal{H} + \alpha\mathcal{I})f = \mathcal{H}^*g \quad \text{and} \quad (\mathcal{H}^*\mathcal{H} + \alpha\mathcal{D}^*\mathcal{D})f = \mathcal{H}^*g,$$

where $\mathcal{I}$ is the identity operator and $\mathcal{D}^*\mathcal{D}$ is the Laplacian operator.

2.2. Neumann Boundary Condition

The usual way of formulating the model with the zero boundary condition[1] will produce ringing effect at the boundary of the reconstructed image, see the numerical results in Bose and Boo[2] . We therefore propose to use the Neumann boundary condition, i.e., the scene immediately outside the frames are reflection of the original frames at the boundary.

The continuous image model in (2) can be discretized by rectangular rule and approximated by a discrete image model as follows. Let $\mathbf{g}$, $\mathbf{f}$ and $\mathbf{H}$ be respectively the discretization of g, f and $\mathcal{H}$ using a lexicological ordering. For simplicity, we discuss the case $L = 2$ here. Other cases can be derived similarly. For $L = 2$, under the zero boundary condition, the blurring matrix corresponding to the (l_1, l_2)-th sensor can be written as

$$\mathbf{H}_{l_1 l_2} = \mathbf{H}^x_{l_1 l_2} \otimes \mathbf{H}^y_{l_1 l_2}$$

where $\mathbf{H}^x_{l_1l_2}$ is the $M_1 \times M_1$ tridiagonal matrix

$$\mathbf{H}^x_{l_1l_2} = \frac{1}{2}\begin{pmatrix} 1 & h^{x+}_{l_1l_2} & & & \\ h^{x-}_{l_1l_2} & 1 & \ddots & & \\ & \ddots & \ddots & \ddots & \\ & & \ddots & 1 & h^{x+}_{l_1l_2} \\ & & & h^{x-}_{l_1l_2} & 1 \end{pmatrix}.$$

Here $h^{x\pm}_{l_1l_2} = \frac{1}{2} \pm \epsilon^x_{l_1l_2}$. The $M_2 \times M_2$ blurring matrix $\mathbf{H}^y_{l_1l_2}$ is defined similarly. We remark that the condition numbers of $\mathbf{H}^x_{l_1l_2}$ and $\mathbf{H}^y_{l_1l_2}$ are of $O(M_1^2)$. For $L > 2$, the matrices $\mathbf{H}^x_{l_1l_2}$ and $\mathbf{H}^y_{l_1l_2}$ are band matrices with bandwidth $L+1$.

Under the Neumann boundary condition, $\mathbf{H}^x_{l_1l_2}$ and $\mathbf{H}^y_{l_1l_2}$ are still tridiagonal matrices, but the entries on the upper left corner and the lower right corner are changed. The resulting matrix, denoted by $\tilde{\mathbf{H}}^x_{l_1l_2}$ and $\tilde{\mathbf{H}}^y_{l_1l_2}$ are given by

$$\tilde{\mathbf{H}}^x_{l_1l_2} = \frac{1}{2}\begin{pmatrix} 1+h^{x-}_{l_1l_2} & h^{x+}_{l_1l_2} & & & \\ h^{x-}_{l_1l_2} & 1 & \ddots & & \\ & \ddots & \ddots & \ddots & \\ & & \ddots & 1 & h^{x+}_{l_1l_2} \\ & & & h^{x-}_{l_1l_2} & 1+h^{x+}_{l_1l_2} \end{pmatrix}.$$

The matrix $\tilde{\mathbf{H}}^y_{l_1l_2}$ can be similarly derived. The blurring matrix corresponding to the (l_1, l_2)-th sensor under the Neumann boundary condition is

$$\tilde{\mathbf{H}}_{l_1l_2} = \tilde{\mathbf{H}}^x_{l_1l_2} \otimes \tilde{\mathbf{H}}^y_{l_1l_2}.$$

Our discretization problem becomes:

$$(\tilde{\mathbf{H}}^*\tilde{\mathbf{H}} + \alpha\mathbf{R})\mathbf{f} = \tilde{\mathbf{H}}^*\mathbf{g} \tag{3}$$

where

$$\tilde{\mathbf{H}} = \sum_{l_1=0}^{L-1}\sum_{l_2=0}^{L-1} \mathbf{D}_{l_1l_2}\tilde{\mathbf{H}}_{l_1l_2}. \tag{4}$$

Here $\mathbf{D}_{l_1l_2}$ are diagonal matrices with diagonal elements equal to 1 if the corresponding component of $\mathbf{g}$ comes from the (l_1, l_2)-th sensor and zero otherwise. In (3), $\mathbf{R}$ is the discretization matrices corresponding to the regularization functional $\mathcal{R}(f)$.

2.3. Cosine Transform Preconditioners

Let $\mathbf{C}_n$ be the $n \times n$ discrete cosine transform matrix, i.e. the (i,j)-th entry of $\mathbf{C}_n$ is given by

$$\sqrt{\frac{2-\delta_{i1}}{n}}\cos\left(\frac{(i-1)(2j-1)\pi}{2n}\right), 1 \le i, j \le n,$$

where δ_{ij} is the Kronecker delta. Note that the matrix-vector product $\mathbf{C}_n x$ can be computed in $O(n \log n)$ operations, see Sorensen and Burrus.[9] For an $m \times m$ block matrix $\mathbf{B}$ with the size of each block equals to $n \times n$, the cosine transform preconditioner $c(\mathbf{B})$ of $\mathbf{B}$ is defined to be the matrix $(\mathbf{C}_m \otimes \mathbf{C}_n)^T\Lambda(\mathbf{C}_m \otimes \mathbf{C}_n)$ that minimizes

$$||(\mathbf{C}_m \otimes \mathbf{C}_n)^T\Lambda(\mathbf{C}_m \otimes \mathbf{C}_n) - \mathbf{B}||_F$$

in Frobenius norm[3] . Clearly, the cost of computing $c(\mathbf{B})^{-1}y$ for any vector y is $O(mn \log mn)$ operations. For banded matrices, like the one we have in (4), the cost of constructing $c(\mathbf{B})$ is of $O(mn)$ only[3] .

When there is no subpixel displacement error, the matrix $\tilde{\mathbf{H}}_{l_1l_2}$ are the same for all l_1 and l_2. Thus the blurring matrix $\tilde{\mathbf{H}}$ can be written as

$$\tilde{\mathbf{H}} = \tilde{\mathbf{H}}^x \otimes \tilde{\mathbf{H}}^y$$

where for $L = 2$, $\tilde{\mathbf{H}}^x$ is an $M_1 \times M_1$ tridiagonal matrix:

$$\frac{1}{4}\begin{pmatrix} 3 & 1 & & & \\ 1 & 2 & 1 & & \\ & \ddots & \ddots & \ddots & \\ & & 1 & 2 & 1 \\ & & & 1 & 3 \end{pmatrix}$$

and $\tilde{\mathbf{H}}^y$ is an $M_2 \times M_2$ matrix with the same structure. It is easy to show that in this case, the matrices $\tilde{\mathbf{H}}^x$ and $\tilde{\mathbf{H}}^y$ can be diagonalized by $\mathbf{C}_{M_1}$ and $\mathbf{C}_{M_2}$ respectively. Thus $\tilde{\mathbf{H}}$ can be diagonalized by $\mathbf{C}_{M_1} \otimes \mathbf{C}_{M_2}$.

When there are subpixel displacement errors, the blurring matrix $\tilde{\mathbf{H}}$ is almost the same as that without errors, but with some entries slightly perturbed. We thus propose to use the cosine transform preconditioner for the BTTB-like matrix $\tilde{\mathbf{H}}$. Our numerical results show that the cosine transform preconditioners can speed up the convergence much faster than other preconditioners. Since $\tilde{\mathbf{H}}$ is banded, the matrix-vector product $\tilde{\mathbf{H}}x$ can be done in $O((L_1 + L_2)M_1M_2)$, thus the total cost per each iteration is $O((L_1 + L_2)M_1M_2 + M_1M_2 \log(M_1M_2))$ operations.

3. NUMERICAL RESULTS

In this section, we illustrate the effectiveness of the cosine transform based preconditioners by solving the high-resolution image reconstruction problem with a 2×2 sensor array and a 4×4 sensor array. In the tests, we use the zero vector as the initial guess in the preconditioned conjugate gradient method. The stopping criteria is $||\mathbf{r}^{(j)}||_2/||\mathbf{r}^{(0)}||_2 < 10^{-6}$, where $\mathbf{r}^{(j)}$ is the normal equations residual after j iterations. In the tests, the parameters $\epsilon^{xy}_{l_1 l_2}$ are set to be 0.1.

(i) 2×2 **sensor array**

Here we reconstruct a 128×128 image from four 64×64 images. The source image "Lena" is shown in Figure 9, Image A. It is a woman face with background, and contains a high degree of contrast and detail. We first illustrate the need of regularization for this problem. In Figure 2, the left one is a low resolution image. The right one is the reconstructed image at 9 iteration with $\|f\|_2^2$ as the regularization operator when the PCG method converges. However, when no regularization is used, the PCG method does not converge to a visually recognizable image image. The middle one is the image solution we obtained at 9 iteration. The SNR here is 40dB. We see that all the details of the original image is lost in the middle figure.

Next we test the effectiveness of using Neumann boundary conditions. Figure 3 shows the error of the first row of the image "Lena" recovered by using different boundary conditions. We used SNR=40dB and $R(f) = \|f\|_2^2$. We perform the experiment in the following way: we first generate the random noise, then reconstruct the image by imposing different boundary conditions, the pair of errors (e_z, e_n) is plotted on the graph, where e_z is the error by imposing zero boundary condition and e_n is the error by imposing Neumann boundary condition. We repeat the same experiment for 50 times. In each case the random noise we added into the observed low resolution is different. The optimal regularization parameter is chosen such that it minimize the relative error. Here the relative error of the reconstructed image $\mathbf{f}_c$ to the original image $\mathbf{f}$ is defined as:

$$\frac{\|\mathbf{f} - \mathbf{f}_c\|_2}{\|\mathbf{f}\|_2}.$$

From the graph, we can see that all the points are lying under the diagonal line, which means that the error by imposing the Neumann boundary condition is significantly less than that of the zero boundary condition in all of the cases. In Figure 4, we also show the reconstructed image under the zero boundary condition from the low resolution image in Figure 2 (left). We can compare Figures 2 (right) and 4. It is clear that the hair and the hat are much better reconstructed under the Neumann boundary condition than that under the zero boundary condition. We see that the boundary artifacts under the Neumann boundary condition are less prominent than that under the zero boundary condition.

In Figures 5 and 6, we show the observed and reconstructed images of the image "Lena" for SNR=40dB and 20dB respectively. Here the optimal regularization parameter α is chosen. We see from Figures 5c, 5d, 6c and 6d that

Image	$\|f\|_2^2$					$\|\mathcal{D}f\|_2^2$				
	α	cos	sin	cir	none	α	cos	sin	cir	none
A	2.7×10^{-3}	9	19	48	74	7.1×10^{-4}	9	18	47	70
B	1×10^{-2}	7	14	24	38	1.9×10^{-3}	7	14	27	42
C	2.4×10^{-2}	7	12	17	28	7.1×10^{-3}	6	11	16	26

Table 1. No. of iterations with optimal α and $L = 2$.

Image	$\|f\|_2^2$					$\|\mathcal{D}f\|_2^2$				
	α	cos	sin	cir	none	α	cos	sin	cir	none
A	1.1×10^{-2}	6	24	33	44	4.1×10^{-3}	6	27	35	48
B	8.1×10^{-3}	6	27	35	43	2.6×10^{-3}	6	32	41	49
C	5.6×10^{-2}	5	14	16	21	1.7×10^{-2}	5	16	18	26

Table 2. No. of iterations with optimal α and $L = 4$.

the hair and the hat are much better restored than the observed high resolution image (Figures 5b, 6b). In order to compare the performance of different regularization methods, we show the relative errors of the reconstructed images. The relative errors for $\|f\|_2^2$ and $\|\mathcal{D}f\|_2^2$ are almost the same. Visually, their reconstructed images also look similarly.

(ii) 4×4 **sensor array**

We perform the same test with the same scenes as in (i), but for a 4×4 sensor array. We use sixteen 32×32 images as the low-resolution images. The reconstructed image is of resolution 128×128. Figures 7–8 show the observed and reconstructed images with SNR=40dB and 20dB respectively. Again, the hair and the hat are much better restored in Figures 7c, 7d, 8c and 8d than those in Figures 7b and 8b. The optimal α is chosen in the testing. Again, the functionals $\|f\|_2^2$ and $\|\mathcal{D}f\|_2^2$ perform more or less the same when optimal α is chosen.

Finally, we test the convergence performance of the cosine transform based preconditioners. We will apply our method on 3 different 128×128 scenes, see Figure 9. Tables 1 show the performance of different preconditioners with $R(f) = \|f\|_2^2$ and $\|\mathcal{D}f\|_2^2$. The SNR here is 40dB. In the table, α that minimizes the relative error is chosen. We test the best α up to 2 significant digit. In the tables, "cos", "sin", "cir", and "none" denote respectively the cosine transform preconditioner, the sine transform preconditioner,[5] the T. Chan circulant preconditioner[11] and no preconditioner. We see from the tables that the cosine transform preconditioner converges significantly faster than the other preconditioners. Table 2 show the performance of different preconditioners with different regularization functions. Optimal α is used in the table. The SNR is 40dB. Again, the cosine transform preconditioner is the best.

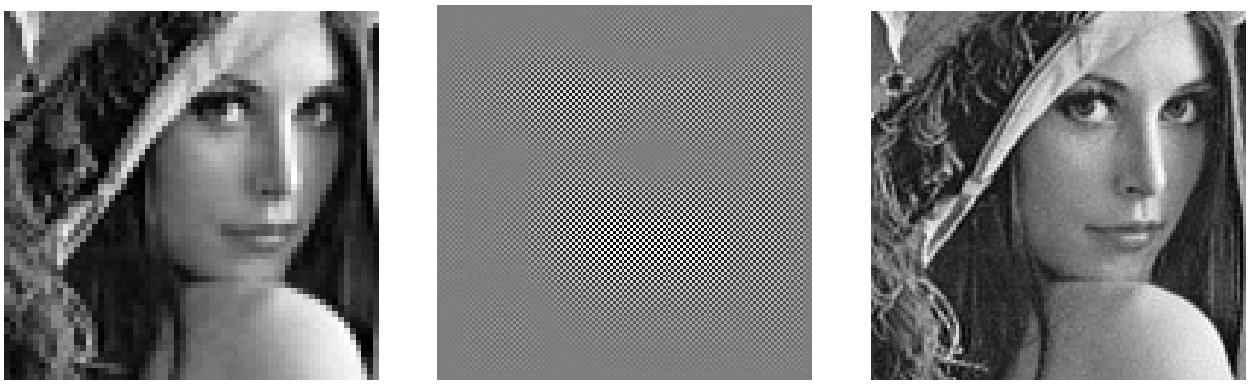

Figure 2. Low resolution 64 x 64 image (left), reconstructed 128 x 128 image (middle) without regularization (at 9 iter.) and (right) with regularization (at 9 iter under the Neumann boundary condition.)

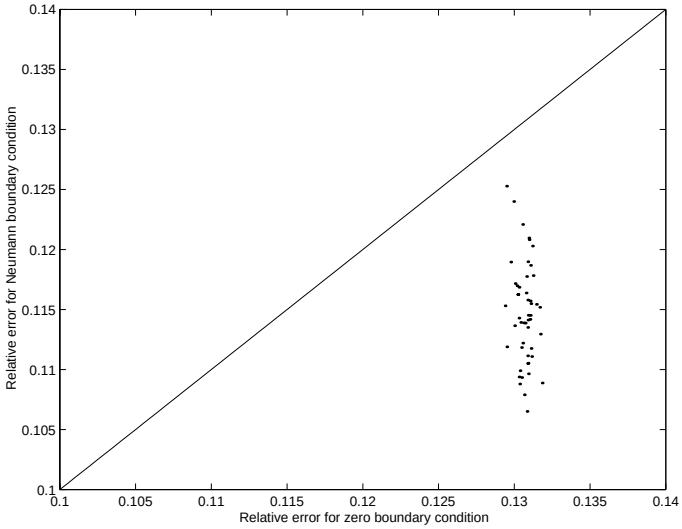

Figure 3. Errors by zero boundary conditions and Neumann boundary conditions.

Figure 4. Reconstructed 128 x 128 image under the zero boundary condition.

$L = 2$, **SNR = 40db**

Fig. 5a. Low resolution 64 x 64 image from the (0,0) sensor.

Fig. 5b. Observed high-resolution 128 x 128 image, rel. err. $= 1.301 \times 10^{-1}$.

Fig. 5c. Reconstructed 64 x 64 image by αI regularization, rel. err. $= 1.194 \times 10^{-1}$.

Fig. 5d. Reconstructed 128 x 128 image by $\alpha\Delta$ regularization, rel. err. $= 1.156 \times 10^{-1}$.

$L = 2$, **SNR = 20db**

Fig. 6a. Low resolution 64 x 64 image from the (0,0) sensor.

Fig. 6b. Observed high-resolution 128 x 128 image, rel. err. $= 1.502 \times 10^{-1}$.

Fig. 6c. Reconstructed 128 x 128 image by αI regularization, rel. err. $= 1.476 \times 10^{-1}$.

Fig. 6d. Reconstructed 128 x 128 image by $\alpha\Delta$ regularization, rel. err. $= 1.497 \times 10^{-1}$.

$L = 4$, **SNR = 40db**

Fig. 7a. Low resolution 32 x 32 image from the (0,0) sensor.

Fig. 7b. Observed high-resolution 128 x 128 image, rel. err. $= 1.861 \times 10^{-1}$.

Fig. 7c. Reconstructed 128 x 128 image by αI regularization, rel. err. $= 1.624 \times 10^{-1}$.

Fig. 7d. Reconstructed 128 x 128 image by $\alpha\Delta$ regularization, rel. err. $= 1.696 \times 10^{-1}$.

$L = 4$, **SNR = 20db**

Fig. 8a. Low resolution 32 x 32 image from the (0,0) sensor.

Fig. 8b. Observed high-resolution 128 x 128 image, rel. err. $= 1.932 \times 10^{-1}$.

Fig. 8c. Reconstructed 128 x 128 image by αI regularization, rel. err. $= 1.765 \times 10^{-1}$.

Fig. 8d. Reconstructed 128 x 128 image by $\alpha\Delta$ regularization, rel. err. $= 1.811 \times 10^{-1}$.

Figure 9. Original 128 × 128 images: Image A (left), Image B (middle) and Image C (right).

4. ACKNOWLEDGMENTS

The work of Raymond Chan was supported by Hong Kong Research Grants Council Grant No. CUHK 4207/97P. Tony Chan was supported by ONR under grant N00014-96-1-0277 and NSF under grant DMS 96-26755. Michael Ng was supported by HKU CRCG grant nos. 335/024/0011 and 10201939/17474/25500/301/01.

REFERENCES

1. H. Andrew and B. Hunt, *Digital Image Restoration*, Prentice-Hall, New Jersey, 1977.
2. N. K. Bose and K. J. Boo. "High-resolution image reconstruction with multisensors", to appear in International Journal of Imaging Systems and Technology.
3. R. H. Chan, T. F. Chan and C. K. Wong. "Cosine transform based preconditioner for total variation minimization problems in image processing", *Iterative Methods in Linear Algebra*, **II(3)**, *IMACS Series in Computational and Applied Mathematics, Proceedings of the Second IMACS International Symposium on Iterative Methods in Linear Algebra, Bulgaria*, pp. 311–329, 1995.
4. R. H. Chan and M. K. Ng. "Conjugate gradient method for Toeplitz system", *SIAM Review,* **38**, pp. 427–482, 1996.
5. R. H. Chan and C. K. Wong. "Sine Transform Preconditioner for Elliptic Problems", *Numer. Linear Algebra Applic.*, **4**, pp. 351-368, 1997.
6. E. Kaltenbacher and R. C. Hardie. "High resolution infrared image reconstruction using multiple, low resolution, aliased frames", *Proc. of IEEE 1996 National Aerospace and Electronic Conf. NAECON* **2**, pp. 702–709, 1996.
7. S. P. Kim, N. K. Bose and H. M. Valenzuela. "Recursive reconstruction of high resolution image from noisy undersampled multiframes", *IEEE Trans. on Acoust., Speech, and Signal Process,* **38(6)**, pp. 1013–1027, 1990.
8. R. R. Schultz and R. L Stevenson. "Extraction of high-resolution frames from video sequences", *IEEE T. Image Proces.*, **5(6)**, pp. 996–1011, 1996.
9. H. Sorensen and C. Burrus, "Fast DFT and convolution algorithms", *Handbook of Signal Processing*, edited by S. Mitra and J. Kaiser, New York, Wiley.
10. A. M. Tekalp, M. K. Ozkan and M. I. Sezan, "High-resolution image reconstruction from lower-resolution image sequences and space-varying image restoration", *In Proc. IEEE Int. Conf. Acoust., Speech, and Signal Process,* **III**, pp. 169–172, San Francisco, CA, March 1992.
11. T. F. Chan and J. A. Olkin. "Circulant preconditioners for Toeplitz-block matrices", *Numer. Algo.,* **6**, pp. 89–101, 1994.
12. R. Y. Tsai and T. S. Huang. "Multiframe image restoration and registration", *Advances in Computer Vision and Image Processing,* **1** pp. 317–339, 1984.